

AFRC Industrial Combustion Symposium
September 10-12, 2022
Greenville, SC

**Capturing the Effect of Near-and Far-Field Dynamics on
the Combustion Efficiency of Multi-point Ground Flares**

Jennifer P. Spinti (jennifer.spinti@utah.edu)

Sean T. Smith (sean.t.smith@utah.edu)

Philip J. Smith (philip.smith@utah.edu)

Jebin Elias (jebin.elias@utah.edu)

The University of Utah, Salt Lake City, UT 84112

Jeremy Thornock (jthornock@gmail.com)

Consultant, Salt Lake City, UT 84108

Marc Cremer (cremer@reaction-eng.com)

Minmin Zhou (zhou@reaction-eng.com)

Reaction Engineering International, Salt Lake City, UT 84047

1 Abstract

Multi-point ground flares are frequently used in scenarios where flare gas flow rates can be high and pollution (noise, light, smoke) needs to be minimized. We have applied Arches, a large eddy simulation (LES) tool that we have developed for capturing the dynamics of flares (turbulent mixing, local combustion efficiency (CE), etc.) and the impact of those dynamics on the quantities of interest (overall CE, heat flux to the surroundings, etc.), to multi-point ground flares. We use a handoff strategy to resolve the flow field in the near-burner region, coarsen the solution at a handoff plane, and then introduce the handoff plane outputs as source terms at the location of the flare tips in a multi-point ground flare mesh. Using this methodology, we perform large eddy simulations of the John Zink steam-assisted SKEC multi-point ground flare test series (SN1) described in Marathon Petroleum Company's Flare Consent Decree¹.

Our handoff approach incorporates one-way coupling only; there is no feedback from the flow field back to the source terms injected at the flare tip. It is a compromise solution that allows us to compute the far-field flow dynamics of flares located adjacent to each other while incorporating the flow field generated by the fine-scale resolution of the flare tip. We will show the impact of the degree of coarsening (fine scale to multi-point flare scale), the location of the handoff plane, the location of the flare tips relative to each other, and the wind speed/direction on the computed overall CE. With this tool, we will be able to investigate effects such as cross-lighting and other interactions amongst multiple flares.

2 Introduction

Multi-point ground flares are frequently employed in systems with high-pressure waste streams (≥ 15 psig) to produce smokeless burning at a low operating cost². As one of three main flare types used in the refining and chemical process industries (single-point and enclosed flares are the other two)², they have been the subject of previous analysis in American Flame Research Committee (AFRC) meetings. At the 2015 AFRC meeting, Ian Fischer discussed the design considerations for purchasers of multi-point ground flares, including flare staging and capacity, burner design, and vent gas composition³. Smith et al.⁴ analyzed heat flux to structures surrounding a multi-point ground flare using a computational fluid dynamics model developed for flares.

The work we present in this paper builds on a multi-fidelity approach to modeling multi-point ground flares that was introduced at the 2020 AFRC meeting⁵. The specific case study we target in this work is a series of three John Zink steam-assisted flares operating at high turndown. Ground flares operate in this mode the majority of the time with full utilization only occurring during process upsets. The data used in this work were collected at the John Zink Flare Facility as part of Marathon Petroleum Company's Flare Consent Decree (as recorded August 30, 2012)¹. We performed the multi-fidelity simulations (both near-burner and far-field) for this work using Arches/Uintah, a large eddy simulation (LES)

tool developed at the University of Utah for capturing the dynamics of flares and other reacting fluid flow systems⁶.

3 Flare Configuration and Data

We obtained most of the information for our analysis from the Marathon report¹. This report did not have detailed information about flare tip geometry nor the experimental configuration of the flare tips, so we deduced what we could from photographs and data in the report and inferred the rest. We determine the sensitivity of overall combustion efficiency ($CE_{overall}$), the quantity of interest or QOI, to some of these assumptions in this paper.

We created detailed geometry files of the flare tip and then utilized those same files for both our near-flare-tip and far-field simulations. The flare tip surface area for the vent gas exit matched the 4.64 in^2 reported for the exit area. Based on the photographs in Fig. 1 and other information, we located the three flare tips along a horizontal line and spaced them 0.91 m apart for the base case. We used outlet boundary conditions for all faces that were not wind inlets (i.e. no ground planes), so the height of the flare tips off the ground was not a variable that needed to be accounted for.



Fig. 1. Configuration of three SKEC flares. (left) View of flares on test pad. (right) Three SKEC flares burning Tulsa natural gas. Images obtained from *Performance Test of Steam-Assisted and Pressure Assisted Ground Flare Burners with Passive FTIR – Garyville* by Clean Air Engineering¹.

The simulations we performed were all variations of the first SKEC test (test 1, replicate 1); see Clean Air, p. 49¹. The combined vent gas flow rate for the three flare tips was 60 lb/hr (0.00756 kg/s), the combined steam flow rate was 130 lbs/hr (0.01638 kg/s), and the measured wind speed was 5 mph (2.2352 m/s). In addition to these input variables, other data collected included wind direction, CE computed from Passive Fourier Transform Infrared Spectroscopy (PFTIR) measurements, and flare gas composition and net heating value (NHV).

In a previous paper, we performed a Bayesian analysis of CE using the PFTIR line-of-sight measurements and results from 20 simulations of a single SKEC flare⁷. The output of that analysis was a set of predicted distributions (e.g. CE with uncertainty) of overall

CE (the actual CE integrated over the entire surface area of the flare) as a function of NHV in the combustion zone (NHV_{cz}). In this paper, we move from a single-flare regime to the three-flare regime of the experiment using a multi-fidelity scaling procedure as described next.

4 Multi-Fidelity and Multi-Flare Framework

We briefly described our first attempt at developing this framework in Cremer et al.⁵. This framework provides a way to interface fine-detailed simulations (over a smaller domain) with coarser simulations (on a much larger domain). We capture near-flare-tip dynamics with a localized domain and communicate that information to a second simulation of the larger-scale mixing using a handoff approach described below. This capability is particularly useful for LES of flares since, just slightly downstream of the tip, it is only the largest eddies that dominate the dynamics of the flow and determine the coupling of mixing and reaction of the air and fuel. Since Arches/Uintah is built on a static, Cartesian mesh, this multi-fidelity framework offers a way to perform a mesh refinement calculation with one-way coupling.

4.1 Fine-Scale Simulations of Near-Tip Region

The first step is to perform fine-scale LES simulations of the near-flare-tip region. We performed three simulations on Ash, a 4000-core machine at the University of Utah’s Center for High Performance Computing (CHPC). The largest case ran on 2688 cores. The base case was a 0.3m x 0.3m x 0.35m domain with 1 mm resolution. There was no crosswind nor reaction (fluid flow only) in this case. The crosswind case had a 5.0 mph (2.2352 m/s) crosswind at the x- face of the domain, a 0.4m x 0.3m x 0.35m domain, and 1 mm resolution. We ran the case with reaction in a 0.3m x 0.3m x 0.4m domain at 1 mm resolution. Figures 2 and 3 show the steam and fuel mass fraction fields at a single time slice in the three simulations. The impact of the crosswind is evident.

The second step is to time average the important simulation data and then define a cutting plane that will serve as the handoff location to the coarse level simulation. We created time-averaged fields of velocity in the vertical (z) direction, enthalpy, fuel mass fraction, and steam mass fraction; we averaged over the last 0.5 s of data in each simulation (the stationary-state region). Our first cutting plane was at $z = 0.1$ m, a location 10 cm above the exit plane of the vent gas. Based on sensitivities noted in a preliminary round of far-field simulations, we then created a second set of handoff data at the vent gas exit plane ($z = 0.09$ m). At these two vertical locations, we extracted data for all four variables from a subset of the plane that captures the local dynamics of the vent gas and steam flows; in this case, the subset is a 0.24m x 0.24m square.

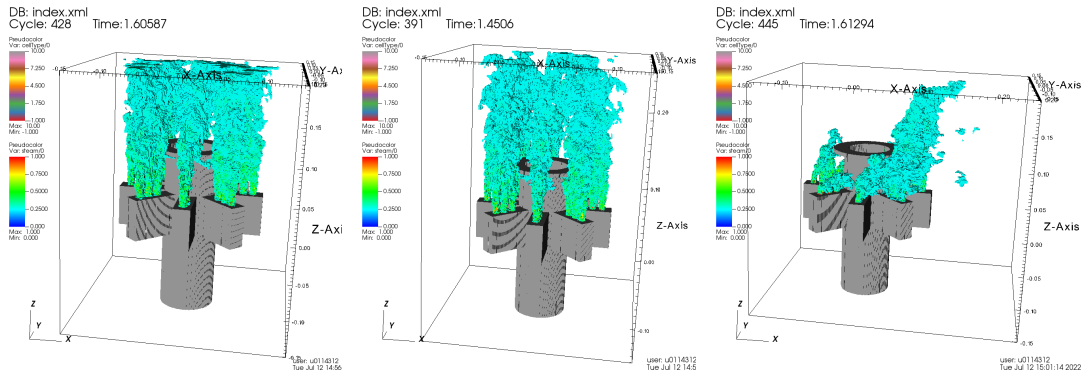


Fig. 2. Steam mass fraction in LES simulations of SKEC burner. (left) Base case, (middle) case with reaction, (right) case with crosswind through x- plane.

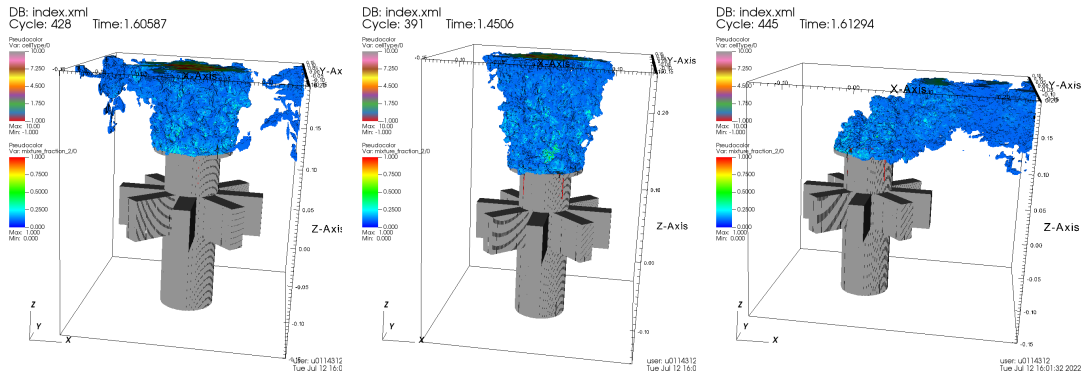


Fig. 3. Fuel mass fraction in LES simulations of SKEC burner. (left) Base case, (middle) case with reaction, (right) case with crosswind through x- plane.

4.2 Coarsening the Fine-Scale Data

The third step is to coarsen the extracted data from the fine-scale simulations in a conservative manner to match the resolution of the coarse mesh. For a prescribed fine-to-coarse ratio, we integrate each variable field (vent gas mass flux, steam mass flux, momentum flux, enthalpy flux) over all of the fine-scale cells within the coarse-scale cell to obtain the coarse-grid flux value for that cell and then repeat the process over all the coarse-grid cells in the 0.24m x 0.24m square. After coarsening, we scale the vent gas and steam mass flow rates to the experimental values. While this scaling is not conservative with respect to the fine-scale handoff data, the scaling step is necessary to avoid introducing extra vent gas and steam mass into the system as the mass flow rates at the cutting plane are different than the mass flow rates at the inlet boundary of the fine-scale simulation due to recirculating eddies. Table 1 compares the various mass flow rates and energy rate before and after coarsening and scaling.

Table 1. Mass balance from fine to coarse scale (10:1 ratio) at the $z = 0.09$ m (vent gas exit) cutting plane.

Component	Fine	Coarse	Coarse with scaling	Experiment
Total mass flow (kg/s)	0.03616	0.03616	0.03616	
Total fuel flow (kg/s)	0.003038	0.003154	0.002520	0.002520
Total energy rate (J/s)	-14316	-14850	-14850	
Total steam flow (kg/s)	0.0085377	0.008793	0.005460	0.005460

This procedure results in a set of coarsened data over the domain of the subset. Figures 4 and 5 show the steam and vent gas mass flux fields respectively. Figure 4 specifically shows the impact of the degree of coarsening. Figure 5 illustrates the influence of the cross wind. The top-row plots are from a cutting plane located 10 cm above the vent gas exit. The wind creates a handoff plane with an asymmetric fuel mass flux across the vent gas exit. The higher fuel concentrations are in the downwind direction where, in the far-field simulation, turbulent mixing enhances the reaction rate. The bottom-row plots are from a cutting plane at the vent gas exit. The effect of the crosswind is muted at this location, resulting in roughly symmetric vent gas flux across the exit. This is a more desirable condition for the handoff files as discussed in Section 5.

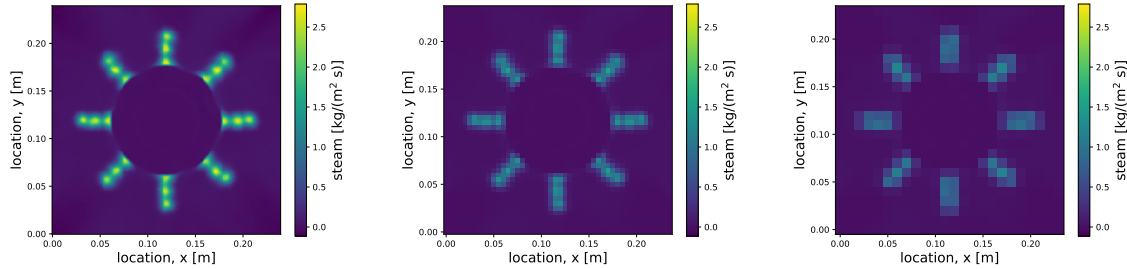


Fig. 4. Steam mass flux field for SKEC flare tip at handoff plane between fine- and coarse-mesh simulations. Cutting plane is at $z = 0.09$ m. (left) Fine scale (1 mm), (middle) coarsened scale (5 mm), (right) coarsened scale (1 cm).

4.3 Far-Field Simulations

The fourth step is to use the coarsened data as a boundary from which fluxes of mass, momentum and energy are injected into the coarse, far-field simulations. Using Arches/Uintah, we constructed an array of three SKEC burners as described in Section 3. At each of the flare tip locations, we defined internal (to the domain) boundary conditions for steam and vent gas, momentum, and energy fluxes using the same set of handoff files at each location.

We then performed a suite of LES simulations on the Ash cluster at CHPC to test sensitivity of $CE_{overall}$ to various uncertain parameters. There are many uncertain parameters

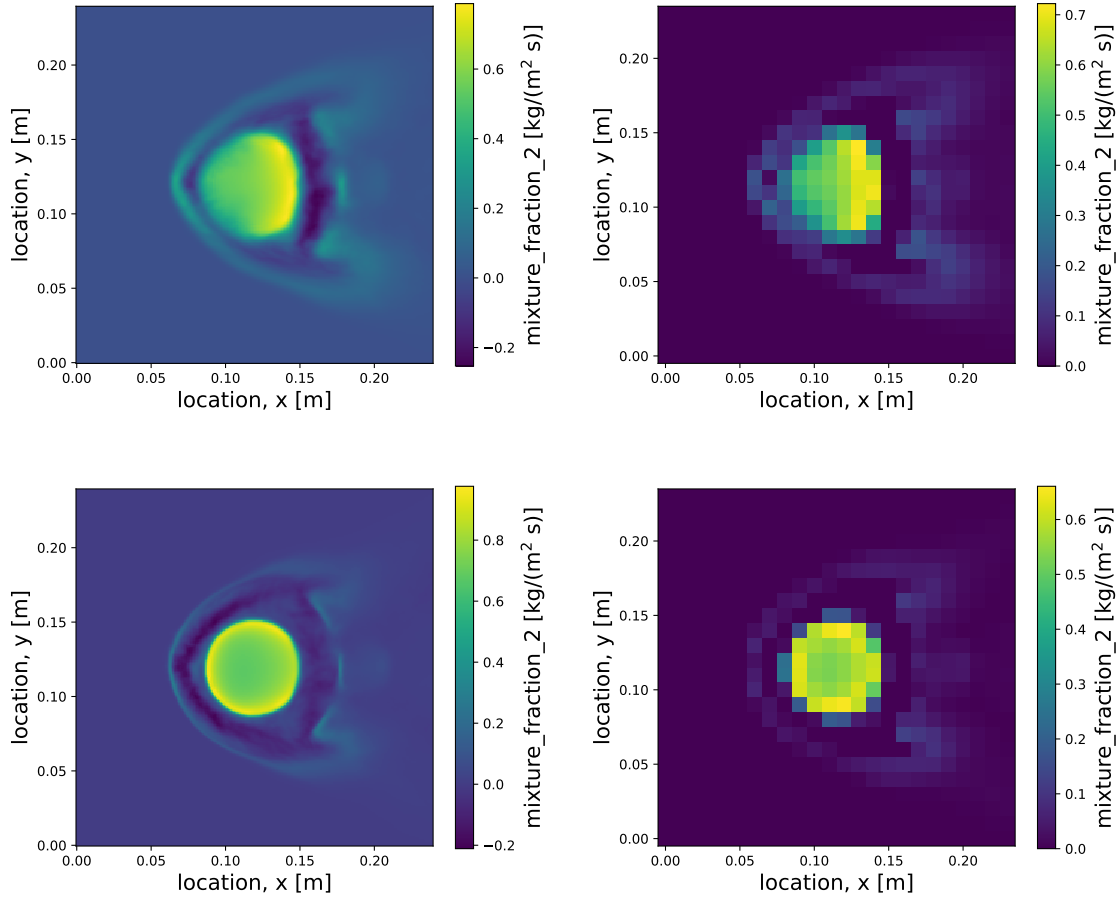


Fig. 5. Vent gas mass flux field for SKEC flare tip at handoff plane between fine- and coarse-mesh simulations. Fine-scale resolution (left) is 1 mm, coarse-scale (right) is 1 cm. Top row uses cutting plane at $z = 0.1$ m. Bottom row uses cutting plane at $z = 0.09$ m.

in this system: model, scenario (experimental inputs and geometry), numerical, instrument model (measurement), and handoff (location of handoff plane, degree of coarsening, scaling, etc.). We explored the impact of several uncertain scenario and instrument parameters in previous work with a single flare⁷. In this paper, we investigate the sensitivity of $CE_{overall}$ to parameters related to the handoff procedure and to the three-flare configuration including location (cutting plane) where the handoff procedure is performed, coarsening ratio (numerical parameter), wind speed and direction, the conditions in the near-field simulation used for the handoff, and the spacing of the flare tips (an unknown scenario parameter).

For the base case, we used a 10:1 coarsening ratio, corresponding to 1 mm resolution for the fine-scale simulation and 1 cm resolution for the three-flare simulation. The computational domain was 2.6 m x 2.6 m x 1.5 m. The wind (5 mph or 2.235 m/s) was perpendicular to the horizontal line of the three flare tips. The handoff location was the vent

gas exit plane ($z=0.09$ m) and the handoff files were generated from the near-burner simulation with no crosswind and no reaction (cold flow). To initiate combustion, we inserted a pilot flame at each flare tip that ran continuously during the simulation. This configuration may be different than the experimental set-up, where there appears to be only one pilot for all three flare tips. We determined the pilot fuel flow rate from Table 2.3.2-1 in the Clean Air report¹, which gives a "pilot rate (per pilot)" of 50 scfh (assumed to be vent gas). We computed the air flow rate as that required for stoichiometric combustion. We ran the case for 24 hours on 600 cores to generate sufficient data to perform a stationary-state analysis. The initial transient exits the domain after 3 s as seen in Figure 6.

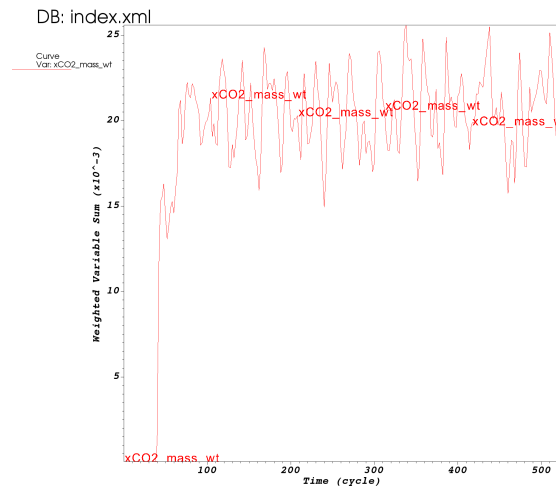


Fig. 6. Base case integrated CO_2 mass flow rate (kg/s) at downstream exit plane of simulation.

Figure 7 shows the volume-rendered temperature and vorticity fields for this base case at one time step. For these wind conditions and flare tip spacing, there is no interaction among the plumes. We performed additional simulations with flare spacing of 0.51 m and with wind entering the domain at a 45° angle. Figures 8 and 9 show the volume-rendered temperature and vorticity fields from these simulations. There is still no plume interaction for either of these configurations, but additional shifts in wind direction or relative locations of the flare tips will result in such interactions.

5 Combustion Efficiency Results and Discussion

The QOI for our sensitivity analysis is $CE_{overall}$. It is the integrated value of CE over the surface that contains the multi-point ground flare and the downstream effluent where reaction is still occurring. We define it as

$$CE_{overall} = \frac{\phi_{CO_2}}{\phi_{CO_2} + \phi_{CO} + \phi_{HC}} \quad (1)$$

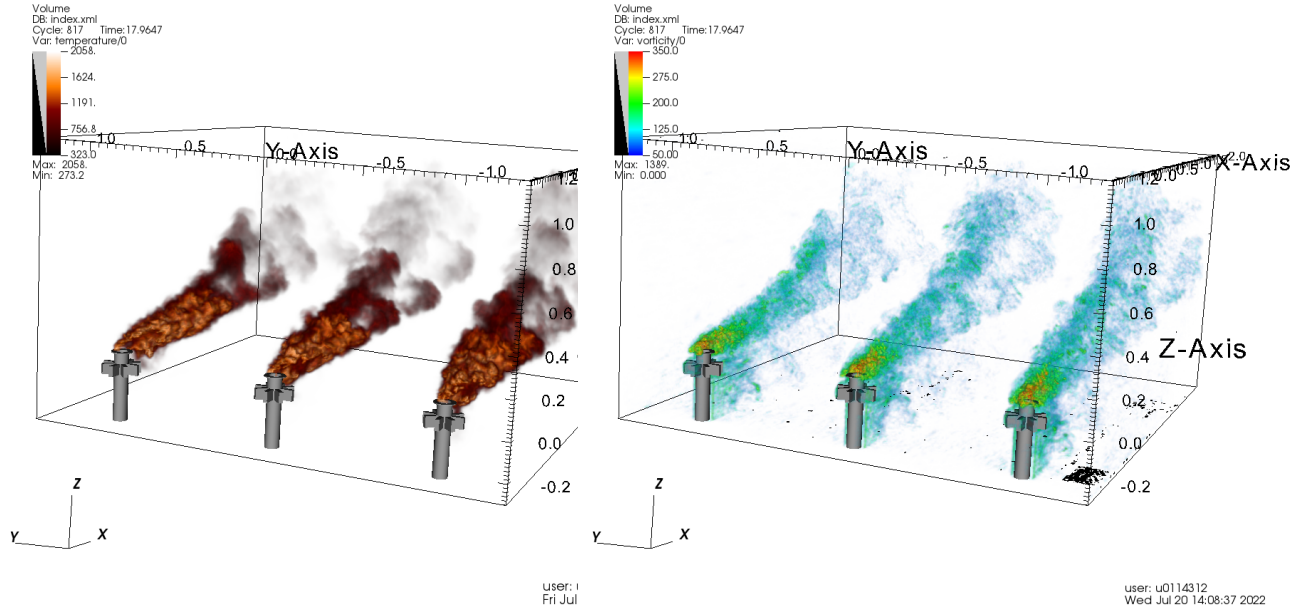


Fig. 7. Volume rendered images (left - temperature, right - vorticity) of the coarse-level, base case simulation using the fine-level information via a handoff plane (10:1 coarsening ratio).

where ϕ_{CO_2} is the combined flux of CO_2 (kg/s) passing through all of the surfaces, ϕ_{CO} is the combined flux of CO , and ϕ_{HC} is the combined flux of unreacted vent gas. In our instrument model for $CE_{overall}$, the surface is defined by the domain boundaries. We create time-averaged plots ($\Delta t = 5s$) for each of the flux components ($x_{CO_2}\rho v$, etc.), take a weighted sum of these components on each face to get a scalar value of flux (kg/s), sum up the total flux for each component across all faces, and then apply Eq. 1.

We ran a series of simulations to test sensitivity to various uncertain parameters and then applied our instrument model for $CE_{overall}$ to the simulation output. All cases were run out to a minimum of 10 s of simulation time. The results are presented in Table 2. The "Handoff condition" label in the table refers to fine-scale simulation from which the handoff data is extracted; see Section 4.1.

We note that the $CE_{overall}$ values in the table are for relative comparison only as they do not include the parametric nor the latent uncertainties. Also, we performed a similar suite of simulations with a handoff plane 10 cm above the vent gas exit. The effects of the cross-wind at this location in the fine-scale simulation produce an asymmetry (see Fig. 5) that strongly impacts the downstream mixing and reaction. This impact is seen in the $CE_{overall}$ results from the base case (0.944) compared with the handoff condition of 2.235 m/s cross-wind (0.977) at $z = 0.1$ m. The purpose of our multi-fidelity approach is to leverage the output from the fine-scale simulation for a large number of far-field multi-flare simula-

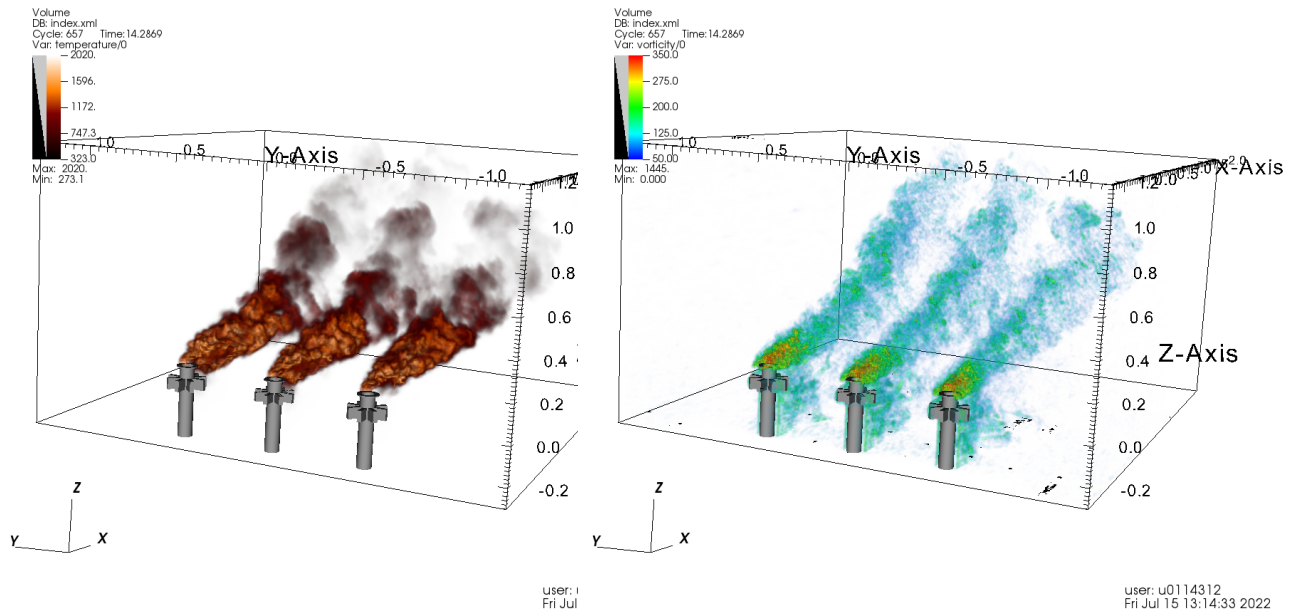


Fig. 8. Volume rendered images (left - temperature, right - vorticity) of the coarse-level simulation with flare tip spacing of 0.51 m (10:1 coarsening ratio).

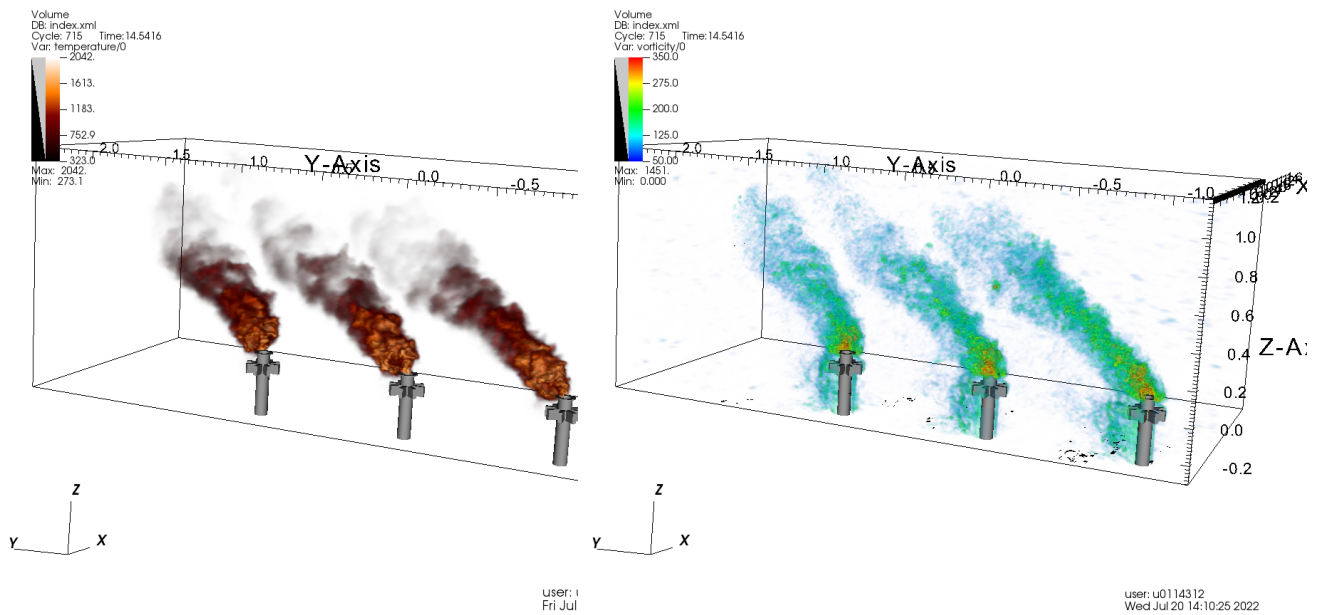


Fig. 9. Volume rendered images (left - temperature, right - vorticity) of the coarse-level simulation with 5 mph (2.235 m/s) wind at 45° (10:1 coarsening ratio).

Table 2. Parametric sensitivity of $CE_{overall}$. Handoff plane is at vent gas exit ($z = 0.009$ m). The approximation to $CE_{overall}$ measured experimentally using a PFTIR is 0.977.

Δ between burners	Wind condition	Coarsening ratio	Handoff condition	$CE_{overall}$
0.91 m	2.235 m/s, 90°	10:1	Non-reacting, no crosswind	0.920
0.91 m	2.235 m/s, 45°	10:1	Non-reacting, no crosswind	0.907
0.91 m	2.235 m/s, 90°	10:1	Non-reacting, 2.235 m/s crosswind	0.929
0.91 m	2.235 m/s, 90°	10:1	Reacting, no crosswind	0.941
0.71 m	2.235 m/s, 90°	10:1	Non-reacting, no crosswind	0.918
0.51 m	2.235 m/s, 90°	10:1	Non-reacting, no crosswind	0.911
0.91 m	2.235 m/s, 90°	7:1	Non-reacting, no crosswind	0.945
0.91 m	2.235 m/s, 90°	5:1	Non-reacting, no crosswind	0.947
0.91 m	0.1 m/s, 90°	10:1	Non-reacting, no crosswind	0.842

tions. Hence, our objective is to reduce the sensitivity of the handoff procedure to scenario parameters such as wind speed and direction that would require additional fine-scale simulations to cover the operational space of the flare. By selecting the handoff plane at the vent gas exit, the crosswind impact is diminished; $CE_{overall}$ for the base case is 0.920 and for the crosswind handoff condition is 0.929. Therefore, these handoff files can be applied to multi-flare simulations over the range of wind conditions observed during the experiment.

The lack of plume interaction for the flare-tip spacing and crosswind directions tested (see Fig. 8 and Fig. 9) is reflected in $CE_{overall}$ values that do not show much sensitivity to either of these parameters. Nevertheless, Fig. 9 indicates that for crosswind directions $< 45^\circ$, plume interaction is likely to occur.

The effect of a numerical parameter, mesh resolution, is seen by comparing $CE_{overall}$ of the base case with a 10:1 coarsening ratio (0.920) to the 7:1 (0.945) and 5:1 (0.947) cases. The mixing rate, and thus the combustion reaction rate, changes with mesh resolution (Δx); we resolve all rates at this scale and above. For coarse mesh resolutions, only the larger-size eddies are resolved. We observe the importance of local mixing in the resolved turbulent eddies by comparing these results to those in the absence of a crosswind (wind speed = 0.1 m/s) where $CE_{overall} = 0.842$. While these data indicate that a mesh resolution of 7 mm is sufficient, there are computational advantages to running with a coarser mesh ($\Delta x = 1\text{cm}$ requires 600 cores while $\Delta x = 7\text{mm}$ requires 1568 cores). Ideally, we can adjust the physics (the combustion model) to reduce the sensitivity to mesh resolution. In future work, we will use the SKEC multi-point ground flare data to learn more about the parameters in the combustion model, optimize them for this system, and determine the appropriate scale for mixing. We will also consider using the same combustion model in the fine-scale simulation given the sensitivity to reaction in the handoff condition.

The phenomena of cross lighting and continued burning in the absence of a pilot flame require the appropriate resolution for the commensurate mixing and reaction rates. We turned off the three pilots in both the base case and the 5:1 coarsening ratio case to de-

termine what resolution is adequate. With the base case, the resolved, large-scale eddies pushed the hot, reacting gases quickly out of the reaction zone, extinguishing the flames almost immediately. With the $\Delta x = 5mm$ case, the middle flare tip remained ignited while the flare tips on the side were extinguished at a slower rate than the $\Delta x = 1cm$ case. This result suggests that the mesh-resolution threshold for computing these phenomena given the current combustion model is slightly less than 4 mm.

6 Conclusions

We have demonstrated a framework that uses a multi-fidelity approach to performing LES simulations of multi-point ground flares. The framework couples a fine-scale simulation of the near-flare-tip region for a single flare with a far-field simulation of a multi-point ground flare using a handoff-plane approach with a coarsening ratio defined by the user. We have applied this approach to a three-flare configuration of SKEC burners and tested the sensitivity of the computed $CE_{overall}$ to various parameters. Because the flares plumes are non-interacting under the tested conditions for wind speed/direction and distance between the flare tips, there is no impact on $CE_{overall}$ for these parameters. The coarsening ratio (i.e. mesh resolution) directly affects the mixing and reaction rate, resulting in $CE_{overall}$ changing from 0.920 to 0.945 between $\Delta x = 1cm$ and $\Delta x = 7mm$.

Acknowledgments/Disclaimer

This material is based upon work supported by the U.S. Department of Energy, Office of Science, under Award Number DE-SC0017039. The authors wish to thank Dan Pearson and Scott Evans at Clean Air Engineering for answering our many questions related to the flare test data.

This paper was prepared as an account of work sponsored by an agency of the United States Government. Neither the United States Government nor any agency thereof, nor any of their employees, makes any warranty, express or implied, or assumes any legal liability or responsibility for the accuracy, completeness, or usefulness of any information, apparatus, product, or process disclosed, or represents that its use would not infringe privately owned rights. Reference herein to any specific commercial product, process, or service by trade name, trademark, manufacturer, or otherwise does not necessarily constitute or imply its endorsement, recommendation, or favoring by the United States Government or any agency thereof. The views and opinions of authors expressed herein do not necessarily state or reflect those of the United States Government or any agency thereof.

References

- [1] Clean Air Engineering. Performance test of steam-assisted and pressure assisted ground flare burners with passive ftir – garyville. Technical report, Marathon Petroleum

Company, LP, 2013. Project No: 12082.

- [2] Adam Bader, Jr. Charles E. Baukal, and Wes Bussman. Selecting the proper flare systems. *Chemical Engineering Progress*, pages 45–50, July 2011.
- [3] Ian M. Fischer. Considerations when specifying multipoint ground flares. In *2015 AFRC Industrial Combustion Symposium*, pages 1–8, 2015. September 9-11.
- [4] Joseph D. Smith and Robert Jackson, Ahti Suo-Anttila, Kerby Hefley, Zach Smith, Doug Wade, Doug Allen, and Scot Smith. Radiation effects on surrounding structures from multi-point ground flares. In *2015 AFRC Industrial Combustion Symposium*, pages 1–12, 2015. September 9-11.
- [5] Marc Cremer, Minmin Zhou, Dave Wang, and Jeremy Thornock. Hardening of arches for commercial simulation of industrial flares: A program update. In *2020 AFRC Virtual Industrial Combustion Symposium*, pages 1–22, 2020. October 19-21.
- [6] M. Berzins and J. Luitjens and Q. Meng and T. Harman and C. Wight and J. Peterson. Uintah: A scalable framework for hazard analysis. *Proceedings of the 2010 TeraGrid Conference; Pittsburgh*, pages 1–3, 2010.
- [7] Jebin Elias, Jennifer P. Spinti, Sean T. Smith, Philip J. Smith, Jeremy N. Thornock, Marc Cremer, and Minmin Zhou. A Bayesian Approach to Quantifying the Uncertainty of Combustion Efficiency Measurements in Flares. In *American Flame Research Committee 2021 Industrial Combustion Symposium*, October 2021.